Available online at www.sciencedirect.com
ScienceDirect
Journal of Magnetic Resonance 188 (2007) 216–230
JMR Journal of Magnetic Resonance
www.elsevier.com/locate/jmr

Optimal control based NCO and NCA experiments for spectral assignment in biological solid-state NMR spectroscopy

Cindie Kehlet [a], Morten Bjerring [a], Astrid C. Sivertsen [a,1], Torsten Kristensen [a], Jan J. Enghild [a], Steffen J. Glaser [b], Navin Khaneja [c], Niels Chr. Nielsen [a,*]

[a] Center for Insoluble Protein Structures (inSPIN), Interdisciplinary Nanoscience Center (iNANO), University of Aarhus, Langelandsgade 140, DK-8000 Aarhus C, Denmark
[b] Department of Chemistry, Technische Universtät München, 85747 Garching, Germany
[c] Division of Applied Sciences, Harvard University, Cambridge, MA 02138, USA

Received 2 April 2007; revised 2 June 2007
Available online 7 July 2007

Abstract

We present novel pulse sequences for magic-angle-spinning solid-state NMR structural studies of ^{13}C,^{15}N-isotope labeled proteins. The pulse sequences have been designed numerically using optimal control procedures and demonstrate superior performance relative to previous methods with respect to sensitivity, robustness to instrumental errors, and band-selective excitation profiles for typical biological solid-state NMR applications. Our study addresses specifically ^{15}N to ^{13}C coherence transfers being important elements in spectral assignment protocols for solid-state NMR structural characterization of uniformly ^{13}C,^{15}N-labeled proteins. The pulse sequences are analyzed in detail and their robustness towards spin system and external experimental parameters are illustrated numerically for typical ^{15}N–^{13}C spin systems under high-field solid-state NMR conditions. Experimentally the methods are demonstrated by 1D $^{15}N \rightarrow {}^{13}C$ coherence transfer experiments, as well as 2D and 3D ^{15}N,^{13}C and ^{15}N,^{13}C,^{13}C chemical shift correlation experiments on uniformly ^{13}C,^{15}N-labeled ubiquitin.

Keywords: Optimal control based optimization; Dipolar recoupling; NCO; NCA; NCOCX; 2D, 3D assignment; Sample heating; Ubiquitin

1. Introduction

Biological solid-state NMR spectroscopy has evolved tremendously during the past few years, now clearly demonstrating its capability for atomic-resolution structural analysis of peptides or proteins immobilized by their presence in aggregated structures (e.g., fibrils) or associated to biological membranes [1–13]. These achievements have been based on years of work establishing the necessary instrumentation, pulse sequence elements, such as dipolar recoupling experiments for rotating samples, and refinements in the sample preparation procedures. The newest biological applications not only indicate good prospects for biological solid-state NMR, they also induce new demands to the solid-state NMR methods. When coping with relatively large line widths, primarily by correlations through ^{13}C and ^{15}N dimensions of multiple-dimensional experiments, issues like resolution and sensitivity become critical. Typically, several 2D and 3D experiments are required to solve structures even for proteins with substantially less than 100 residues. The sensitivity/resolution problem obviously becomes more severe for larger proteins.

When analyzing uniformly ^{13}C,^{15}N-isotope labeled proteins with solid-state NMR, it proves useful to have access to NCO- and NCA-type 2D/3D experiments providing

* Corresponding author. Address: Center for Insoluble Protein Structures (inSPIN), Interdisciplinary Nanoscience Center (iNANO), Department of Chemistry, University of Aarhus, Langelandsgade 140, DK-8000 Aarhus C, Denmark. Fax: +458 6196199.
E-mail addresses: ncn@chem.au.dk, ncn@inano.dk (N.Chr. Nielsen).
[1] Present address: Francis Bitter Magnet Laboratory, Massachusetts Institute of Technology, Cambridge, MA 02139, USA.

1090-7807/$ - see front matter © 2007 Elsevier Inc. All rights reserved.
doi:10.1016/j.jmr.2007.06.011

correlations between ^{15}N and ^{13}C chemical shifts. The transfer of coherence between ^{15}N and ^{13}C spin species in these experiments may be carried out using double-cross-polarization (DCP) [14], off-resonance [15], ramped [16], adiabatic [17], or phase-alternated [18,19] versions of DCP, or symmetry-based recoupling schemes such as C7 [20] or off-resonance C7 [21]. These schemes are, however, in many respects far from optimal and typically they suffer from one or more of the following problems: (i) Intolerance to rf inhomogeneity, often being a major reason for low transfer efficiencies, (ii) high rf demands on the ^{15}N and ^{13}C channels, which in concert with appropriate ^{1}H decoupling may lead to undesired sample heating, (iii) difficult setup because of very narrow Hartmann–Hahn matching conditions, which also hamper transfer of experimental conditions from sensitive "setup samples" to real protein samples (we note that in some cases, e.g., using DCP, the matching condition is so narrow that even minor instrumental variations in the rf power levels and tuning may give substantial variations in transfer efficiency for identical experiments on a single sample), and (iv) low tolerance towards chemical shift interactions, leading to reduced sensitivity in cases with large chemical shielding anisotropies, unless compensated for by the use of strong rf fields.

These difficulties call for improved experiments such as the recently presented optimal control based version of DCP, the so-called ^{OC}DCP experiment [22], or a recent combination of DCP with improved characteristics from composite rotations, i.e., the COMB DCP experiment [23]. In the design of such experiments, it has been a key element to obtain transfer efficiencies which at least match those of typical γ-encoded recoupling techniques [24], in ideal cases enabling transfer of 73% of the coherence from one spin to another in a powder sample. We note that we in this study do not make any comparison with non-γ-encoded experiments such as TEDOR [25], since these, due to less favorable powder crystallite angle dependency, are associated with theoretical transfer efficiencies in the order of 50% or lower (for broadband experiments, e.g., TEDOR, the sensitivity is often substantially further reduced by distribution of coherence to spins beyond the desired destination spin). For a comparison between DCP, TEDOR, and a γ-encoded TEDOR variant GATE, we refer to Ref. [19]. We also note that coherence transfer between adjacent spins using the recently suggested PAIN-CP experiment [26] did not, in our hands, improve efficiencies in NCA and NCO experiments relative to normal DCP, most likely due to rf inhomogeneity effects and distribution of magnetization to more spins through third spin interactions.

In this paper, we will extend our earlier "model-system based" ^{OC}DCP experiments [22] to biological applications by specifically designing experiments for high-field $^{15}N \rightarrow {}^{13}C_{\alpha}$ (NCA) and $^{15}N \rightarrow {}^{13}C'$ (NCO) transfers in solid proteins under consideration of typical internuclear distances, chemical shielding anisotropies, ranges of isotropic chemical shifts, and rf inhomogeneity. The goal is to provide optimum sensitivity over the relevant range of chemical shifts, while providing experiments which use relatively weak rf fields and which are robust towards variations in the most critical instrumental parameters.

2. Optimal control design of recoupling experiments

Our objective in the use of optimal control theory [27,28] for designing optimal NMR experiments is to derive pulse sequences which in a given time, for a typical nuclear spin system, and under typical experimental conditions provide the highest possible transfer efficiency. This is by no means a different aim than set for many other strategies in numerical pulse sequence design. The major difference is exploitation of the unique capability of optimal control to handle systematic variation of hundreds of free parameters throughout the optimization. This property cannot be found for normal non-linear optimization [29], or more analytical and semi-analytical approaches, where even a handful of free variables may impose severe challenges to the optimization and the time required for this. In these latter cases, it is crucial to have a well-defined problem and an "almost solved solution" (e.g., a pulse sequence scaffold), where the optimization only is used for fine tuning of model variables. This represents a very important difference to optimal control approaches, where one typically does not provide any restraints to the pulse sequence scaffold but instead lets the optimization take advantage of all degrees of freedom by freely varying the amplitudes/phases of all pulses in a multiple-pulse experiment (potentially with specified penalty to the maximum rf amplitudes or other experimental constraints). In this study, we apply the so-called Gradient Ascent Pulse Engineering (GRAPE) method developed with focus on liquid-state NMR by Khaneja, Glaser and coworkers [30–35] and in the context of solid-state NMR by Nielsen and coworkers [22,36–39]. For solid-state NMR applications, the algorithm has been implemented into the SIMPSON software [40] using a conjugate gradient based approach [22].

With our specific aim being optimization of coherence transfer between two hetero-spins I and S (e.g., ^{15}N and ^{13}C), we consider the rotating-frame Hamiltonian

$$H(t) = \omega_I(t)I_z + \omega_S(t)S_z + \omega_{IS}(t)2I_zS_z + H_{\mathrm{rf}}(t), \tag{1}$$

where the first three terms represent the I- and S-spin chemical shifts and the heteronuclear dipolar coupling, while the last term describes the external rf fields

$$H_{\mathrm{rf}}(t) = \omega_{\mathrm{rf}}^{Ix}(t)I_x + \omega_{\mathrm{rf}}^{Iy}(t)I_y + \omega_{\mathrm{rf}}^{Sx}(t)S_x + \omega_{\mathrm{rf}}^{Sy}(t)S_y. \tag{2}$$

Expressions for the time- and orientation dependent frequencies for the internal nuclear spin interactions can be found in, e.g., Ref. [40]. In a setting with a train of N pulses acting consecutively on the initial spin density operator $\rho(0)$, the density operator at time $t_N = T$ (i.e., the chosen length of the sequence) takes the form

$$\rho(T) = \mathrm{U}_N(t_N, t_{N-1}) \ldots \mathrm{U}_2(t_2, t_1) U_1(t_1, t_0) \times \rho(t_0) \mathrm{U}_1^+(t_1, t_0) \mathrm{U}_2^+(t_2, t_1) \ldots \mathrm{U}_N^+(t_N, t_{N-1}), \quad (3)$$

with each propagator defined as $\mathrm{U}(t_{k+1}, t_k) = \exp\left\{-\mathrm{i}\int_{t_k}^{t_{k+1}} \mathrm{H}(t)\,\mathrm{d}t\right\}$. To optimize the transfer efficiency $s(T) = \mathrm{Tr}[\rho(T)C^+]$ for a particular destination operator C (e.g., S^+), we also need to calculate a "back-transformed" operator

$$\lambda(t_j) = \mathrm{U}_{j+1}^+(t_{j+1}, t_j) \ldots \mathrm{U}_N^+(t_N, t_{N-1}) \times C\mathrm{U}_N(t_N, t_{N-1}) \ldots \mathrm{U}_{j+1}(t_{j+1}, t_j), \quad (4)$$

using the same propagators as in Eq. (3). Equipped with the formula in Eqs. (3) and (4), it is possible to describe a gradient which in an iterative fashion modifies the rf field (i.e., the I_x, I_y, S_x, and S_y coefficients) for each pulse (e.g., the pulse j operating in time period Δt_j from t_j to t_{j+1}) according to

$$\omega_{\mathrm{rf}}^q(t_j) \to \omega_{\mathrm{rf}}^q(t_j) + \varepsilon \mathrm{Tr}\{\mathrm{i}\Delta t_j[q, \rho(t_j)]\lambda(t_j)\}, \quad (5)$$

where ε is a small real number. Using this gradient as element in a conjugated gradient based optimization, it is possible to establish a powerful numerical environment for optimal control design of pulse sequences.

The remarkable feature about Eq. (5) is that all $4N$ pulse variables through individual gradients are adjusted in every iteration, and thereby all contributing to a better transfer efficiency. This implies that even with 1000 sets of pulses, i.e., 4000 variables, it is possible to obtain convergence within an acceptable period of time, also in cases of powder samples, with inclusion of contributions from different rf isochromats (for inhomogeneous rf fields), and with contributions from nuclei with different chemical shift parameters. In addition to these parameters and the initial and desired final spin states, it is obviously also necessary to provide an initial guess on the pulse sequence. This may be an earlier proposed pulse sequence, or more typically just a random pulse sequence for which the rf field amplitudes (our control fields) are chosen randomly between given upper and lower limits (either for each pulse in the pulse train or more smoothly by randomly selecting the amplitudes on every, say, fifth pulse and then interpolate these amplitudes to the interleaving pulses).

While the optimal control based approach described above is completely general for problems dealing with optimizing transfer from one state to another on the level of density operators (approaches dealing with optimizations on the level of effective Hamiltonians or propagators can be found in Refs. [30] and [38]), it is obviously the system as described by the internal and external Hamiltonians that may change as reflected in previous papers [22,36–39]. In this paper, we focus on $^{15}\mathrm{N} \leftrightarrow {}^{13}\mathrm{C}$ coherence transfer in MAS NMR of rotating solids with specific attention to $^{15}\mathrm{N} \to {}^{13}\mathrm{C}_\alpha$ (intraresidue) and $^{15}\mathrm{N} \to {}^{13}\mathrm{C}'$ (interesidue) transfer between directly attached nuclei in a polypeptide backbone as illustrated in Fig. 1a. For this purpose, we optimize the pulse sequence element illustrated by the toned boxed in Fig. 1b, in the form of a generalized train of pulses depending on the x- and y-phase rf fields as indicated in Fig. 1c. In the present setup, we have chosen the pulses to be of equal length and the resonance offset to be fixed at the mean isotropic chemical shifts of the specific type of nuclei under consideration, e.g. $^{13}\mathrm{C}_\alpha$. With respect to the latter constraint, we note that sweeping of the offset may be accommodated during the optimization by variations in the rf pulse phases, which is obviously within the limits of the chosen digitalization of the pulses.

In the optimization, it is relevant to consider typical spin system parameters for the given transfer, and known variations in these, to provide "spin-system robust" pulse sequences. For most spin systems of relevance for proteins, this may conveniently be accomplished using the SIMMOL software [41] which on basis of structural coordinates from PDB files [42] may provide typical parameters for the magnitudes and orientations of dipolar couplings and anisotropic shielding tensors. This feature is quite obvious for dipole–dipole couplings which only depend on the internuclear distance and the orientation of the bond vector. For the shielding tensors, it is based on the well-established fact that the magnitudes and orientations of these within protein backbone peptide planes are relatively insensitive to secondary structure, with variations that may be estimated to a good approximation [[41,43–45], and references therein]. Here we base our NCO optimizations on the interaction tensors: $b^{\mathrm{NC}'}/2\pi = 1176\,\mathrm{Hz}$, $\Omega_{\mathrm{PE}}^{\mathrm{NC}'} = (\alpha_{\mathrm{PE}}^{\mathrm{NC}'}, \beta_{\mathrm{PE}}^{\mathrm{NC}'}, \gamma_{\mathrm{PE}}^{\mathrm{NC}'}) = (0°, 90°, 57°)$, $J_{\mathrm{iso}}^{\mathrm{NC}'} = -15\,\mathrm{Hz}$, $\delta_{\mathrm{iso}}^{N} = 120\,\mathrm{ppm}$, $\delta_{\mathrm{aniso}}^{\mathrm{N}} = 99\,\mathrm{ppm}$, $\eta^N = 0.19$, $\Omega_{\mathrm{PE}}^{\mathrm{C}'} = (-90°, -90°, -17°)$, $\delta_{\mathrm{iso}}^{\mathrm{C}'} = 175\,\mathrm{ppm}$, $\delta_{\mathrm{aniso}}^{\mathrm{C}'} = -76\,\mathrm{ppm}$, $\eta^{\mathrm{C}'} = 0.90$, and $\Omega_{\mathrm{PE}}^{\mathrm{C}'} = (0°, 0°, 94°)$. As both chemical shift tensors in this case are fixed to the peptide plane, we initially consider the dominant variation to be the isotropic chemical shifts where we incorporated variations from 100 to 140 ppm for $^{15}\mathrm{N}$ and 168–182 ppm for $^{13}\mathrm{C}'$, which on a 16.4 T (700 MHz for $^1\mathrm{H}$) instrument amounts to variations within ± 1.4 kHz for $^{15}\mathrm{N}$ and ± 1.2 kHz for $^{13}\mathrm{C}'$, when the rf carrier frequencies are placed at the mean isotropic chemical shifts for the involved types of spins. The NCA optimizations were based on (same $^{15}\mathrm{N}$ chemical shift tensor): $b^{\mathrm{NC}\alpha}/2\pi = 890$ Hz, $\Omega_{\mathrm{PE}}^{\mathrm{NC}\alpha} = (90°, 115.3°, 0°)$, $J_{\mathrm{iso}}^{\mathrm{NC}\alpha} = -11\,\mathrm{Hz}$, $\delta_{\mathrm{iso}}^{\mathrm{C}\alpha} = 55\,\mathrm{ppm}$, $\delta_{\mathrm{aniso}}^{\mathrm{C}\alpha} = -20\,\mathrm{ppm}$, $\eta^{\mathrm{Ca}} = 0.43$, and $\Omega_{\mathrm{PE}}^{\mathrm{C}\alpha} = (90°, 90°, 0°)$. In this case, we used a variation of the $^{13}\mathrm{C}_\alpha$ isotropic chemical shifts within 42.5–67.5 ppm, which for a 16.4 T instrument correspond to variations within ± 2.2 kHz around the mean isotropic chemical shift. We note that, in this case, the orientation of the $^{13}\mathrm{C}$ chemical shift tensor may vary somewhat depending on the secondary structure [46], but under conditions of relatively fast sample spinning the precise orientation for this tensor seems not to be critical for the optimizations.

In addition to consideration of the spin-system parameters, it is highly relevant to consider the external manipulations, with the aim of generating sequences being robust to

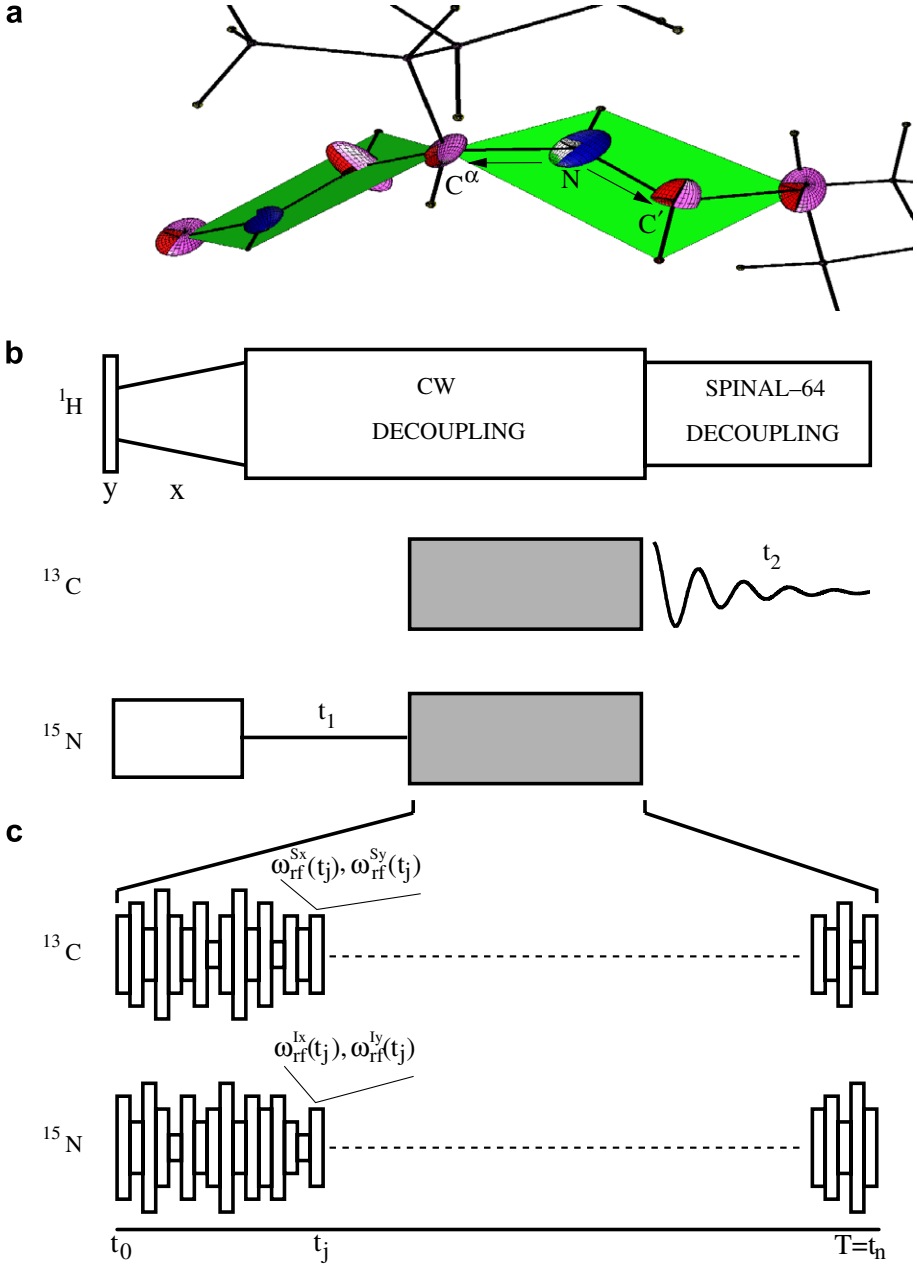

Fig. 1. (a) SIMMOL representation of a peptide fragment indicating the $^{15}N \rightarrow {}^{13}C_{\alpha}$ (NCA) and $^{15}N \rightarrow {}^{13}C'$ (NCO) transfers and typical ^{13}C, ^{15}N chemical shielding tensors relevant for the design of optimal control pulse sequences. (b) Schematic diagram of a typical 2D solid-state NMR triple-resonance experiment for assignment of ^{15}N and ^{13}C chemical shifts with the $^{15}N \rightarrow {}^{13}C$ coherence transfer element marked by toned boxes. (c) Pulse sequence element indicating the x- and y-phase field strengths on the ^{15}N and ^{13}C rf channels which represent our control variables in the design of recoupling experiments providing optimum coherence transfer from time t_0 to time $T = t_n$.

rf inhomogeneity, providing relatively fast excitation, and having low-to-modest rf power consumption to avoid excessive sample heating. We presently assume high-field conditions with 16.4 T equipment (700 MHz for ^{1}H) to ensure optimization over a relevant range of isotropic chemical shifts and to face the increased influence from anisotropic shielding at high fields. We base the investigation on 12 kHz spinning, which represents a good comprise between the lower spinning frequencies typically compatible with broadband symmetry-based recoupling sequences [20,21,47–49] and the ultra-fast spinning situation relying on J-mediated transfer or adiabatic recoupling for $^{13}C \rightarrow {}^{13}C$ transfers [50] while typically using DCP or adiabatic DCP for $^{15}N \rightarrow {}^{13}C$ transfers. We take into consideration 5% Lorentzian rf inhomogeneity (full-width-half-height for the rf distribution function relative to the nominal rf field strength; in the relevant range resembling a 10% Gaussian profile inhomogeneity) which is typical for 2.5–4 mm Bruker probes, and we set an upper limit on the ^{15}N and ^{13}C rf field strengths to 30 kHz. The latter restriction implies that ^{1}H decoupling with less 100 kHz amplitude will readily allow for efficient decoupling—

which for 12 kHz spinning is far from being the case for most symmetry-based CN or RN [20,47–49] recoupling elements.

3. Experimental

^{13}C,^{15}N-labeled ubiquitin was overexpressed in *Escherichia coli* BL21(DE3) cells transformed with pET-21b(+) plasmid encoding for human ubiquitin in M9 minimal medium containing 1 g/l $^{15}NH_4Cl$ and 1 g/l uniformly ^{13}C-enriched glucose. After purification, the protein was dialyzed into a 20 mM Na-citrate buffer at pH 4.1. Microcrystals were grown from a solution containing 10 mg protein in 400 μl buffer gently mixed with 600 μl 2-methyl-2,4-pentanediol (MPD) [7].

Numerical calculations and optimal control based development of pulse sequences were performed on standard Linux PC's using the open-source SIMPSON software package [40] combined with [22] a conjugate gradient version of the GRAPE algorithm [30] as described above. Representative ^{15}N, $^{13}C_\alpha$, and $^{13}C'$ dipolar coupling and chemical shielding tensors and tensor visualization were provided using the open-source software SIMMOL [41] and powder averaging were based on crystallites selected using the REPULSION method [51].

All experiments were performed on a widebore Bruker 700 Avance NMR spectrometer equipped with a standard 4 mm triple-resonance MAS probe. The sample was cooled to approx. −10 °C using an FTS Airjet (FTS Systmes, Inc., Stone Ridge, NY). All experiments used 12 kHz spinning, 4 s repetition time, and ^1H to ^{15}N cross-polarization of duration 800 μs with a 80–100% ramp on ^1H and using rf field strengths of approx. 47 (^1H) and 35 (^{15}N) kHz. Dependent on the applied ^1H–^{13}C and ^1H–^{15}N cross-polarization conditions the overall efficiency of DCP $^1H \rightarrow {}^{15}N \rightarrow {}^{13}C$ transfer relative to direct CP $^1H \rightarrow {}^{13}C$ transfer was in the order of 25% after ensuring that sufficiently strong ^1H decoupling is applied to avoid dissipation to the proton reservoir. This number may at first sight appear low, but can be rationalized in the DCP $^{15}N \rightarrow {}^{13}C$ transfer step due to rf inhomogeneity (with 5% Lorentzian rf inhomogeneity the efficiency of this step drops from 73% to around 35%) and the application of different CP conditions for the $^1H \rightarrow {}^{13}C$ and $^1H \rightarrow {}^{15}N$ CP elements, including losses through broadband-facilitating RAMPs and rf inhomogeneity etc. However, when comparing the performance of the sequences, the only important issue is that the DCP experiment is carefully optimized and sufficient decoupling is applied throughout this element. The 2D NCO/NCA experiments used 148/120 scans for each of the 80/80 t_1 increments with a spectral width of 3.55/3.55 kHz (zero-filled to 1024/1024 points) and with a spectral width of 61.7/62.5 kHz (zero-filled to 4096/4096 points) for the t_2 dimension. Phase-sensitive 2D/3D spectra were obtained using the TPPI protocol [52]. The 3D NCOCX experiment used the same set up and parameters as the 2D NCO experiment followed by a 30 ms DARR element [53] for $^{13}C' \rightarrow {}^{13}C_X$ magnetization, where 'X' indicates all types of ^{13}C in a protein. The DARR element was implemented with ^{13}C $\pi/2$ pulses of 6 μs and the soft pulse amplitude matching the spinning frequency. The t_1 and t_2 dimensions were acquired with 16 and 32 increments, spectral widths of 1.70 and 2.46 kHz, and zero-filling to 64 and 512 points. The t_3 dimension had a spectral width of 67.0 kHz (zero-filled to 8192 points). 240 scans were used for each increment.

4. Results

Using the optimal control based version of SIMPSON with parameters for the internal and external parts of the heteronuclear two-spin Hamiltonian as described above, and assuming the initial operator I_x (^{15}N) and the destination operator S^- (^{13}C), it is possible to derive a pulse sequence which for a given mixing time provides optimum transfer efficiency. In our implementation, the optimizations run in an automated fashion, leading to an optimal pulse sequence. For the practical use, it is relevant to mention that the optimization can be relatively time consuming (from hours to several days on a normal Linux PC), depending on the number of crystallites (typically 20–144 α_{CR}, β_{CR} angles selected using REPULSION [51], 5–10 γ_{CR} angles), the number of rf isochromats (typically 5–10 rf field values weighted according to the inhomogeneity profile, e.g., 5% Lorentzian), the number of offset points (typically in a 2D grid with 4–16 points), the size of the spin system (here a heteronuclear two-spin-1/2 system), and the number of pulses used in the transfer element (typically a train of pulses each of 10 μs duration, which for a 2.4 ms pulse sequence corresponds to 240 pulses on each channel). While optimization of a single sequence may take less than a couple of hours of CPU time, it is much more time demanding to make a large number of optimizations based on random initial pulse sequences to avoid the effect of local extrema and thereby with good likelihood obtain a sequence with the optimal efficiency.

Fig. 2 shows typical optimal control based pulse sequences for NCA and NCO transfers under conditions of high static magnetic field (16.4 T) and sample spinning at 12 kHz. For each of the two transfers, the pulse sequence contains two channels of 240 rf pulses each having a duration of 10 μs, and characterized by a x- and y-phase amplitude (i.e, $\omega_{rf}^{Ix}/2\pi, \omega_{rf}^{Iy}/2\pi, \omega_{rf}^{Sx}/2\pi, \omega_{rf}^{Sy}/2\pi$) represented by solid and dashed lines, respectively, in Fig. 2. To appreciate the overall consumption of rf power, the figures also provide the absolute rf amplitude for each pulse marked by a dot and for each channel a horizontal line representing the average root-mean-square rf power. Addressing the latter point, it is remarkable that the average rf power of the two sequences is in the order 13–17 kHz on both channels, which is substantially lower than the rf fields typically used for DCP, adiabatic DCP, and certainly symmetry-based recoupling experiments. This facilitates efficient ^1H decoupling during the low-γ spin coherence transfer, and reduces the

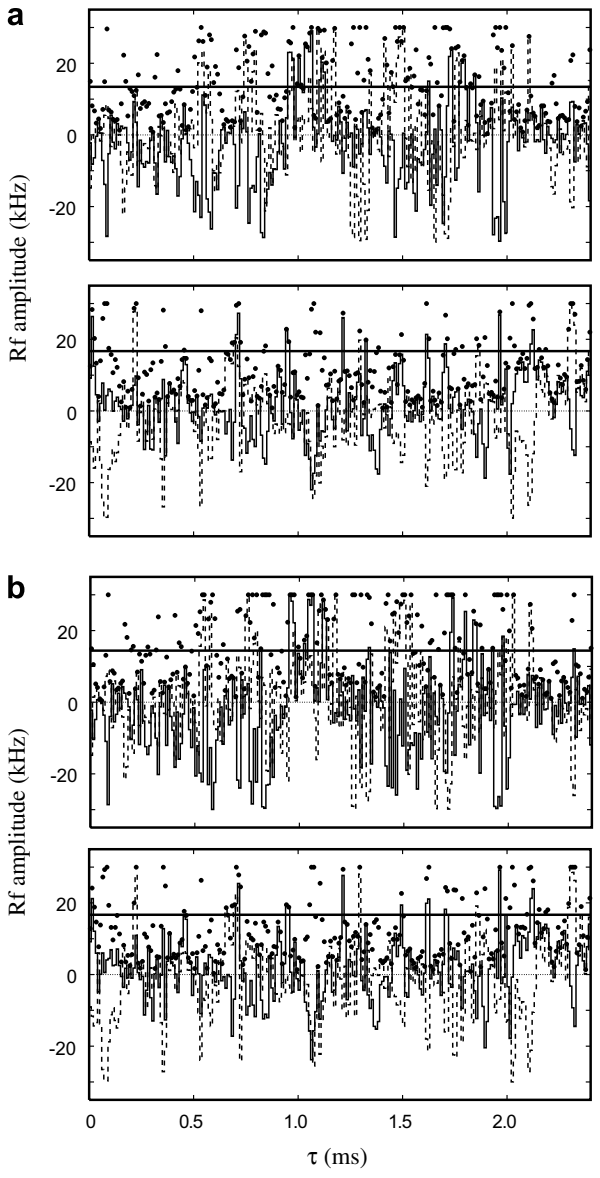

Fig. 2. Optimal control (a) ^{OC}NCA and (b) ^{OC}NCO pulse sequences designed to provide optimum $^{15}N \rightarrow {}^{13}C_{\alpha}$ and $^{15}N \rightarrow {}^{13}C'$ coherence transfer, respectively, between directly bonded nuclei in protein backbones. *x*- and *y*-phase components of the rf field amplitude are marked by solid and dashed lines, respectively, while the absolute amplitude is indicated by dots. The upper panels represent rf irradiation on the ^{13}C channel, while the lower represent irradiation on ^{15}N. The average root-mean-square rf powers are represented by horizontal lines. The sequences are optimized for 12 kHz spinning, a static magnetic field of 16.4 T, 5% Lorentizan rf inhomogeneity, maximum rf field strengths of 30 kHz, and typical parameters for NCA and NCO relevant chemical shift and dipolar coupling tensors in peptides. The amplitudes and phases for the pulse sequences can be found in Supplementary material.

risks of sample heating to be essentially the same as for standard decoupling under acquisition in the direct dimension.

4.1. Numerical analysis of the ^{OC}NCA and ^{OC}NCO experiments

Several parameters are important factors for the performance of the pulse sequences, not only with respect to the overall efficiency of the experiment, but also for the setup and reliability of the pulse sequence throughout time-consuming experiments and for reliable extraction of signal intensities from the resulting multiple-dimensional spectra. In this section, we will by a series of numerical simulations illustrate that the optimal control pulse sequences, in contrast to common reflections, are very robust in most respects and certainly live up to the performance that one should request for in experiments of this kind.

In our preliminary account on optimal control derivation of pulse sequences for ^{15}N to ^{13}C magnetization transfer [22], it was clearly recognized that one of the major problems for DCP-based heteronuclear dipolar recoupling experiments is their sensitivity towards rf inhomogeneity. Exactly this issue rendered the ^{OC}DCP experiments around 50% more efficient than DCP, simply through a better compensation toward inhomogeneous rf fields. Accordingly, our ^{OC}NCA and ^{OC}NCO elements for protein applications under high-field conditions are optimized to compensate for typical rf profiles, as here expressed by a 5% Lorentzian shape. To illustrate the performance of the resulting optimal control sequences and compare this with DCP and adiabatic DCP (with the rf fields, including the adiabaticity parameters, optimized under consideration of the same inhomogeneity), Fig. 3 shows contour plots mapping the ^{15}N to ^{13}C transfer efficiency as function of the inhomogeneity on the two rf channels expressed in terms of factors κ_C and κ_N representing the scaling of the two rf fields relative to their nominal values. The DCP and APCP (adiabatic-passage cross polarization) [17] experiments were optimized numerically based on 12 kHz spinning and rf fields strengths of 33 and 21 kHz on the ^{13}C and ^{15}N rf channels, respectively, with minor readjustments for NCO where the large carbonyl chemical shielding tensor may influence the Hartman–Hahn match condition. The length of the ^{OC}DCP, DCP, and APCP experiments are 2.4, 1.8, and 8 ms, respectively.

From the plots in Fig. 3, it is evident that the ^{OC}NCA and ^{OC}NCO experiments compensate very well for the rf inhomogeneity imposed in the optimizations leading to transfer efficiencies exceeding 60–70% in the relevant regime (for ^{OC}NCO the maximal transfer is 78%) and an overall transfer of 65% when coadding weighted contributions from all isochromats in the case of correlated (i.e., same scaling factor on both channels) 5% Lorentzian inhomogeneity profiles on the two channels. For the DCP and APCP experiments, the maximal transfer efficiencies for the best isochromats are 35% and 65% for NCA/NCO, with an extremely narrow profile (in particular for DCP), and an overall transfer efficiency of 25/29% and 56/55% for NCA/NCO DCP and APCP experiments, respectively, when adding all isochromats in case of 5% Lorentzian inhomogeneity. We note that the optimizations may readily be set up to cover situations with larger inhomogeneity essentially without reducing the efficiency of the OC experiments.

A major concern in the design of optimal coherence transfer schemes for biological applications is the chemical

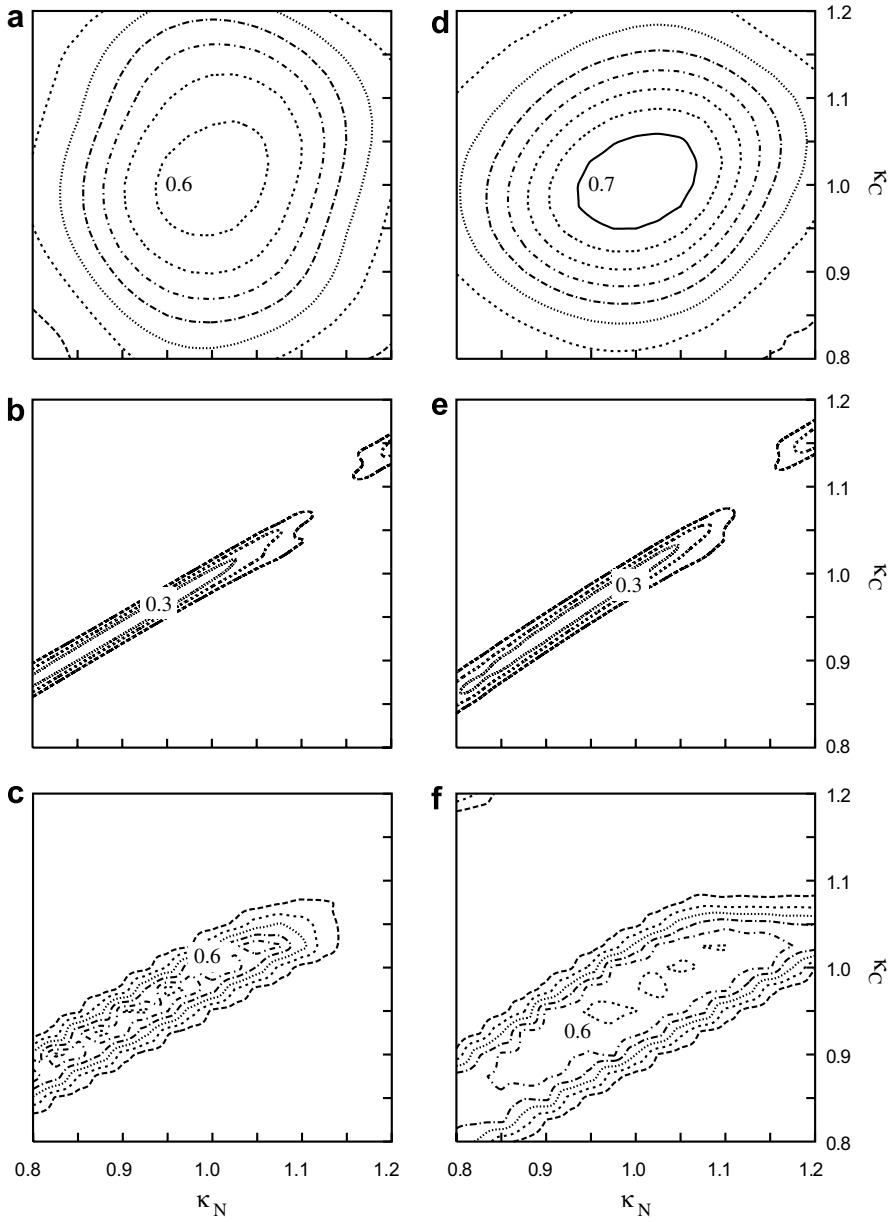

Fig. 3. Contour plots illustrating the sensitivity of (a) ^{OC}NCA, (b) DCP for NCA, (c) APCP for NCA, (d) ^{OC}NCO, (e) DCP for NCO, and (f) APCP for NCO with respect to rf inhomogeneity. The contour levels are equidistant with a separation of 0.1. For the DCP and APCP the nominal rf field strengths are $\omega_{rf}^{N}/2\pi = 21$ kHz and $\omega_{rf}^{C}/2\pi = 33$ kHz.

shift range over which the method works. The method has to be sufficiently broadbanded to ensure transfer of coherence from the initial state to the desired target state for all spin pairs of the same type in the sample independent on their chemical shifts. At the same time, it may for sensitivity, spectral simplicity, digitalization, or rf power consumption reasons be desirable to restrict the transfers to specific bands of chemical shifts instead of using excessively broadbanded experiments. In this study, we focus on band-selective experiments accomplishing specific $^{15}N \rightarrow {}^{13}C_{\alpha}$ and $^{15}N \rightarrow {}^{13}C'$ transfers and not a mixture between the two. Accordingly, the NCA and NCO experiments were optimized to cover 40, 25, and 14 ppm bands (full width) around the isotropic chemical shifts of amide ^{15}N, $^{13}C_{\alpha}$, and $^{13}C'$. The performance of the ^{OC}NCA and ^{OC}NCO sequences with respect to resonance offset are given in Fig. 4, along with comparisons to DCP and APCP. All curves takes into consideration 5% Lorentzian rf inhomogeneity. From the plots, it is clear that optimal control enables design of band-selective excitation schemes with perfect tailoring of the frequency range (here rectangular shapes, but it could be designed to any profile) over which the excitation occurs with an efficiency exceeding 60% while the efficiency rapidly decreases to zero outside this band. We note that the excitation bands of DCP and APCP will never be rectangular shaped and that the efficiencies in the "hot spots" are lower than for the optimal control sequences, in particular for the DCP experiment. For the

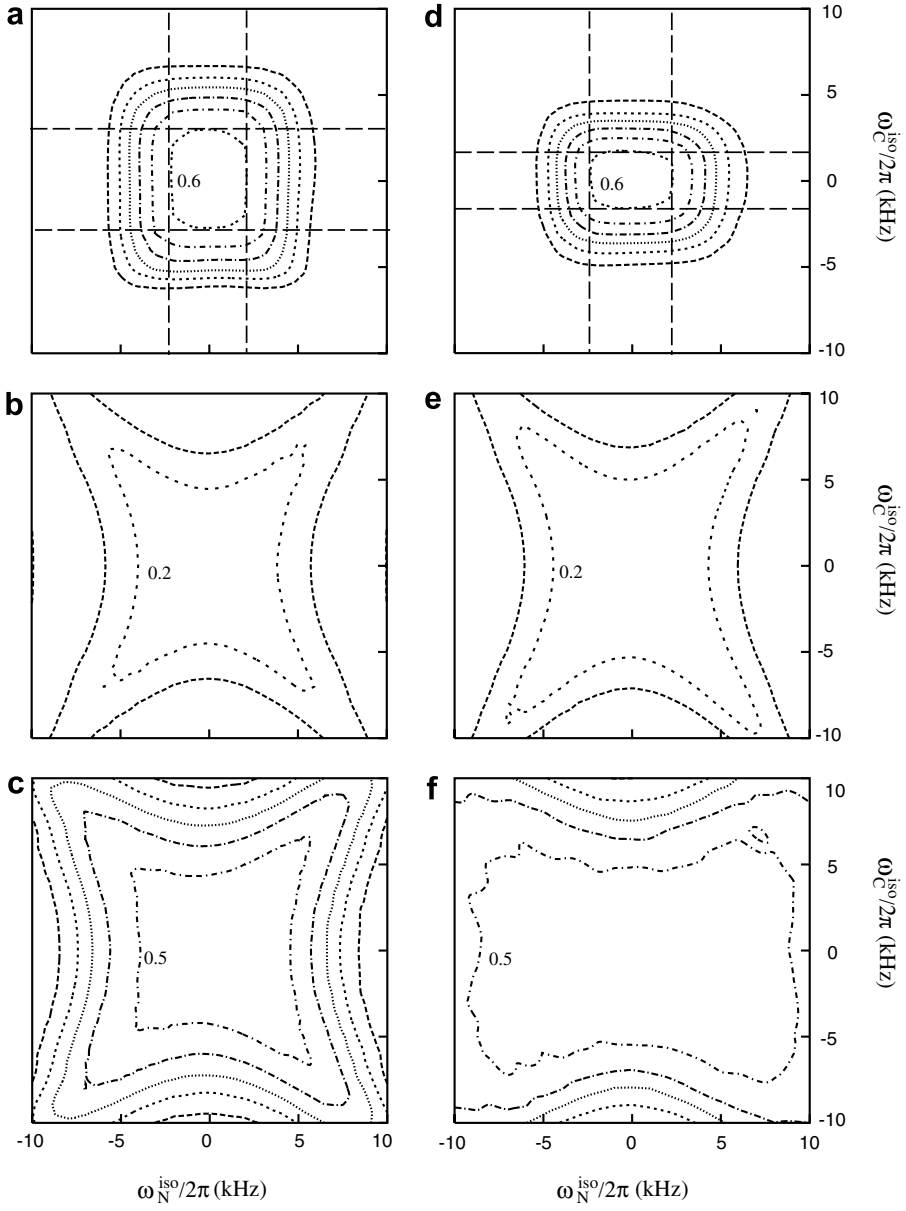

Fig. 4. Contour plots illustrating the sensitivity of (a) ^{OC}NCA, (b) DCP for NCA, (c) APCP for NCA, (d) ^{OC}NCO, (e) DCP for NCO, and (f) APCP for NCO towards resonance offsets (and thereby variation in isotropic chemical shifts) in relevant regions for the two transfers. The contour levels are equidistant with a separation of 0.1. The simulations assume 5% Lorentzian rf inhomogeneity.

latter experiments, the profile can obviously be adjusted by changing the rf field strengths and the parameters for the tangential shape for APCP. However, this has the drawback that, e.g., increase/decrease of the isotropic chemical shift bandwidth will typically scale the bandwidth on both channels simultaneously and may often be associated with increased sensitivity towards chemical shielding anisotropies (in case of decreased rf fields) or result in increased sensitivity to rf inhomogeneity and demands to proton decoupling (and thereby increased sample heating) in case of increased rf fields.

In comparing the quality of the recoupling experiments in terms of sensitivity towards rf inhomogeneity and offsets, it is relevant to emphasize that the favorable performance of the optimal control experiments appears while simultaneously decreasing the demands to the rf power, and thereby associated problems with sample heating. For the ^{OC}NCA and ^{OC}NCO experiments the root-mean-square average $^{13}C/^{15}N$ rf powers are in the order of 14/17 kHz while it is 33/21 kHz for the corresponding DCP and APCP experiments. Taking into account the different lengths of the experiments, this corresponds to relative rf energy factors (i.e., the squared rf field strength multiplied by time accumulated for the full sequence) 0.57/0.32 (optimal control, 2.4 ms), 1/1 (DCP, 1.8 ms), and 4.45/4.44 (APCP, 8 ms) for the $^{13}C/^{15}N$ rf irradiation in NCA experiments. For NCO experiments the corresponding numbers are 0.62/0.40 (optimal control, 2.4 ms), 1/1 (DCP, 1.8 ms),

and 4.05/4.44 (APCP, 8 ms). Considering that irradiation on the ^{1}H channel with an rf field strength is typically 2.5–3 times the rf field strength on the low-γ channel with strongest rf irradiation, it is clear that the most relevant comparison concerns the optimal control experiments and DCP. On the other hand, if extended excitation times are acceptable, it is relevant to consider APCP or probably more favorably optimal control experiments optimized for longer excitation periods.

In Fig. 5, we explore the robustness of the optimal control derived ^{OC}NCA and ^{OC}NCO pulse sequences towards changes in the spinning frequency and the static external magnetic field relative to the parameters used in the optimizations, and compare their performances to that of DCP and APCP. It is evident that the optimal control sequences—as expected—are less tolerant towards variations in the spinning speed than to traditional recoupling experiments, but certainly sufficiently robust to ensure that it is insensitive to any typical variation in the spinning speed using standard solid-state NMR equipment (otherwise, it would have been straightforward to optimize the experiments to compensate for a reasonable variation in the spinning frequency). For more general applications, however, it is also clear that OC sequences are not "scalable" as standard recoupling experiments with respect to substantial changes of the spinning frequency. This was clear already at the stage of the optimizations. Considering the other positive quality factors of the optimal control sequence, we do not consider this a major practical problem. This applies not least when noting that for most applications published so far the spinning speed falls into three categories: (i) low-speed spinning 4–7 kHz dictated by a wish to use recoupling sequences with relatively high rf-to-spinning-speed demands while simultaneously requiring efficient ^{1}H decoupling, (ii) fast spinning 10–14 kHz being dictated by the wish of having less intensity of the carbonyls and aromates going into sidebands, while avoiding the sidebands interfering with the aliphatic region of the spectrum, or (iii) ultra-fast spinning 30–70 kHz to use DREAM [54] or *J*-based TOBSY [50] transfers, or the more recent CMAR [55] experiments. Accordingly we believe that derivation of optimal control sequences for a few selected spinning frequencies will cover the full range of typical applications.

The right-hand column of Fig. 5 illustrates that the optimal control sequence are very robust towards variation in the static magnetic field, and hence can be used with benefit for practically all relevant magnetic fields, provided the chemical shift ranges optimized (along with the sequence) are adequate. It is also clear that the gain relative to the DCP and APCP experiments (optimized numerically for 700 MHz) becomes more pronounced for higher fields, illustrated e.g., by gain factors of 2.49/3.29 and 1.14/1.34 for relative to DCP and APCP in NCA transfers at 700/900 MHz, while the corresponding numbers are 2.25/4.01 and 1.26/1.63 for NCO transfers.

As a final topic in our numerical demonstration of the capability of optimal control recoupling experiments for

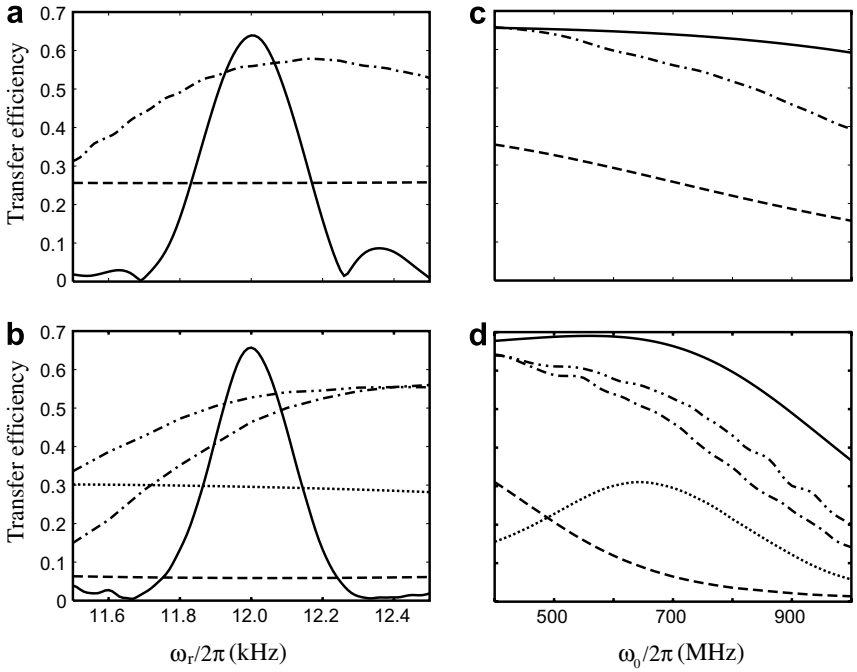

Fig. 5. Numerical simulations illustrating (a and b) spinning speed and (c and d) external magnetic field (in ^{1}H MHz) dependencies for the ^{OC}NCA and ^{OC}NCO experiments in Fig. 2 (solid line) relative to DCP (dashed line; for NCO the dotted line uses $\omega_{rf}^{C}/2\pi = 32$ kHz) and APCP (dash–dot line; for NCO the dash–dot–dot line uses $\omega_{rf}^{C}/2\pi = 32$ kHz) for (a and c) NCA and (b and d) NCO transfers. The DCP and APCP experiments use rf field strengths of $\omega_{rf}^{N}/2\pi = 21$ kHz and $\omega_{rf}^{C}/2\pi = 33$ kHz (if not specified otherwise) with the tangential shape of the adiabatic sequences optimized to provide highest possible efficiency [17].

biological applications, we examine variation in the internuclear distances and the ability of optimal control recoupling experiments to extract information about internuclear distances from excitation profiles. We note that this is not a primary issue for the use in assignment protocols, but more an issue of general interest since dipolar recoupling experiments so far has been proposed/used both for specific transfers and for measurement of dipolar coupling constants. To explore the latter aspect, Fig. 6 shows the transfer efficiency as function of time and as function of dipolar coupling strength for the proposed ^{OC}NCA and ^{OC}NCO experiments. These curves reveal that although the experiments are designed for specific dipolar couplings and for fixed time, it is possible to derive information about internuclear distances from the excitation profiles. This subject is currently under further investigation, with specific focus on the use of optimal control derived pulse sequences for measurement of nuclear spin interactions to probe structure and dynamics.

4.2. Experimental demonstrations for U–^{13}C,^{15}N-ubiquitin

The ultimate tests of the performance of the optimum control experiments involve experimental demonstrations for samples of practical relevance. For this purpose, we have performed a series of 1D, 2D, and 3D experiments on a uniformly ^{13}C,^{15}N-enriched microcrystalline sample of ubiquitin—a small globular protein consisting of 76 amino acid residues. With the aim of conducting experiments with least possible sample heating effects, we restricted the experimental comparison to the relatively short OC and DCP recoupling experiments (2.4 and 1.8 ms, respectively) while leaving out the adiabatic experiments which require very long periods (in the order of 8 ms) with strong rf irradiation (21, 33, and around 100 kHz for the ^{15}N, ^{13}C and ^{1}H channels, respectively).

In Fig. 7, we compare the performance of ^{OC}NCA/^{OC}NCO experiments with the corresponding DCP experiments for $^{15}N \rightarrow {}^{13}C_{\alpha}/{}^{15}N \rightarrow {}^{13}C'$ coherence transfer for ubiquitin at 16.4 T (700 MHz for ^{1}H) and using 12 kHz spinning. The figure is organized with 1D spectra for specific comparison of transfer efficiencies to the left, and 2D ^{15}N,^{13}C chemical shift correlation spectra obtained using the optimal control sequences to the right. Comparing the 1D spectra to the left the ^{OC}NCA and ^{OC}NCO sequences provide gain factors of 1.33 and 1.57 relative to the corresponding DCP experiments, translating into time reduction factors of between 1.8 and 2.5 which obviously serves a useful resource in practical applications. We should note that the experimental gains—although quite substantial—are lower than the theoretically predicted gains, which may be due to several factors currently to be explored. Differences in the specific rf inhomogeneity profiles (e.g., smaller experimental inhomogeneity) could influence the results, likewise may instrumental imperfections such as phase transients play a role. Despite this discrepancy, the 2D spectra support the overall view from the 1D spectra, namely that the sensitivity gain appears uniformly over the NCA and NCO spectra regions and that a spectral quality similar to that previously reported for spectra of uniformly ^{13}C,^{15}N-isotope labeled ubiquitin [7,56,57] has been obtained.

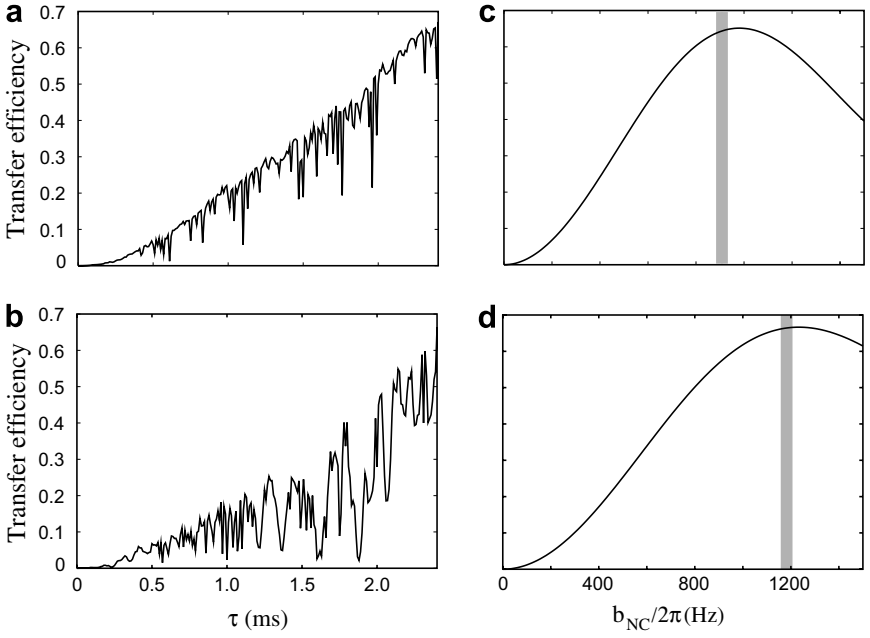

Fig. 6. Transfer efficiency of (a and c) ^{OC}NCA and (b and d) ^{OC}NCO experiments calculated as function of (a and b) the excitation time τ (note that we here address two individual pulse sequences, optimized to be at maximum at the time end-point, rather than probing the maximum achievable efficiency for the various time points—which will require individual optimizations and thereby different pulse sequences for different time points) and (c and d) the dipolar coupling constant $b_{NC}/2\pi$. In latter plots, the vertical bar indicate typical ^{15}N–$^{13}C_{\alpha}$ and ^{15}N–$^{13}C'$ dipolar coupling constants.

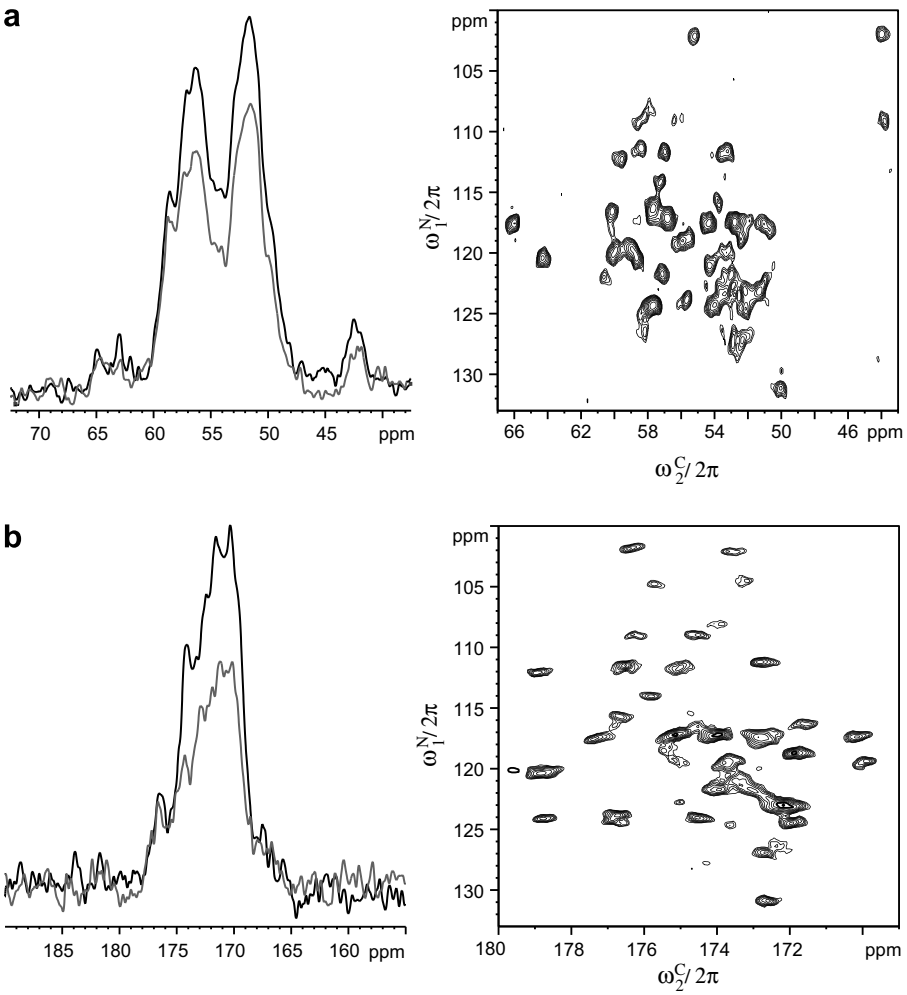

Fig. 7. Experimental 1D (left) and 2D (right) spectra illustrating the performance of (a) $^{15}N \rightarrow {}^{13}C_\alpha$ and (b) $^{15}N \rightarrow {}^{13}C'$ coherence transfer processes for uniformly ^{13}C,^{15}N-labeled ubiquitin obtained using the optimal control ^{OC}NCA (a), ^{OC}NCO (b), and DCP (a and b; left column, grey/lower curves) experiments. The optimal control pulse sequence are illustrated in Fig. 2 and the rf field amplitudes and phases are given in Supplementary material.

With reference to the extensive numerical analysis of the DCP and optimal control recoupling experiments in the previous sections, it seems relevant to explore experimentally the performance of these experiments on ubiquitin and demonstrate the superior performance of the optimal control experiments. For this purpose, Fig. 8 shows the influence of different ^{13}C (Fig. 8a) and ^{15}N (Fig. 8b) rf field scaling factors for DCP (upper row) and ^{OC}NCO (lower row) for the case of $^{15}N \rightarrow {}^{13}C'$ transfer. Indeed, these arrays of 1D spectra of the carbonyl region reveal that the ^{OC}NCO experiment is much more robust to rf inhomogeneity than the DCP experiment not only providing significantly higher sensitivity but also greatly facilitating the experimental setup and long-term stability of the experiments for biological applications.

To experimentally demonstrate the chemical shift specificity of the optimal control designed experiments, Fig. 9 shows a series of 1D $^{15}N \rightarrow {}^{13}C'$ spectra plotted as function of the rf carrier position (i.e., chemical shift offset) for (a) ^{13}C and (b) ^{15}N for the DCP (upper row) and ^{OC}NCO (lower row) for uniformly ^{13}C,^{15}N-isotope labeled ubiquitin. These spectra clearly demonstrate the power of optimal control based procedures in designing experiments with appropriate band-selective excitation profiles covering the region of specific interest (*vide infra*, note that in the pulse sequence optimization, penalty was not given to transfer outside the desired spectral window, implying a smooth fall off, relative to a sharp cutoff that may have been obtained upon incorporating request on zero transfer outside this window in the optimization).

As a final example, Fig. 10 demonstrates the use of the ^{OC}NCO transfer element as a building block in a 3D experiment correlating ^{15}N, $^{13}C'$, and ^{13}C chemical shifts on the ω_1, ω_2, and ω_3 axes in a so-called NCOCX experiment. The pulse sequence is shown schematically in Fig. 10a with an ^{OC}NCO element, following the ^{1}H–^{15}N cross-polarization, transferring magnetization exclusively from ^{15}N to the preceding carbonyl in the protein backbone. The DARR element, consisting of two $\pi/2$ pulses on ^{13}C and a weak rf field (rf field strength matching the rotor frequency) applied to ^{1}H, causes a broadband ^{13}C–^{13}C magnetization transfer facilitating establishment of the desired chemical

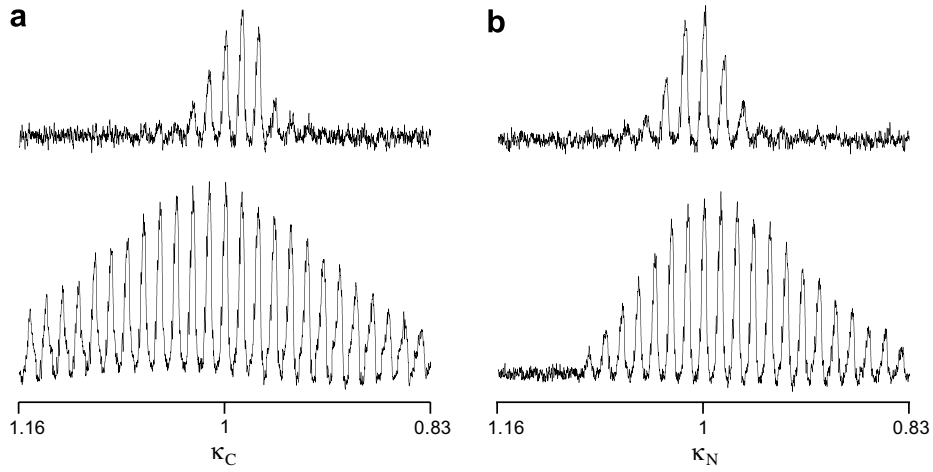

Fig. 8. Experimental 1D spectra (only carbonyl regions are shown) illustrating the performance of $^{15}N \rightarrow {}^{13}C'$ coherence transfer for uniformly ^{13}C, ^{15}N-labeled ubiquitin as function of scaling ($\kappa = 1$ corresponds to the optimal rf fields) of the (a) ^{13}C and (b) ^{15}N rf field strengths applied during the DCP (upper row) and the ^{OC}NCO (lower row) recoupling experiments used for coherence transfer.

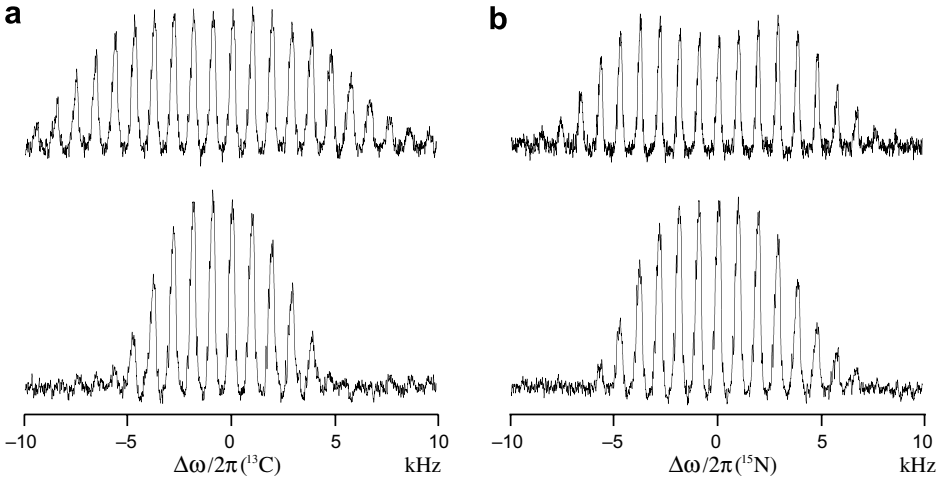

Fig. 9. Experimental 1D spectra illustrating the performance of $^{15}N \rightarrow {}^{13}C'$ coherence transfer for uniformly ^{13}C,^{15}N-labeled ubiquitin as function of ^{13}C (a) and ^{15}N (b) offset during DCP (upper row) and ^{OC}NCO (lower row) recoupling.

shift correlations. Fig. 10b shows the $^{13}C'$ (left) and $^{13}C_\alpha$ (right) regions of the 3D spectrum, while Fig. 10c shows 2D slice elements of the 3D spectrum extracted for $\omega_1/2\pi(^{15}N) = 119.5$ ppm. On these slice elements, three ^{15}N–^{13}CO–$^{13}C_\alpha$ correlations are seen, and the assignments are given.

5. Conclusions

In conclusion, we have in this paper demonstrated the applicability of optimal control theory for numerical optimization of dipolar recoupling experiments with relevance for typical biological solid-state NMR. The optimal control ^{OC}NCA and ^{OC}NCO pulse sequence elements proposed for $^{15}N \rightarrow {}^{13}C_\alpha$ and $^{15}N \rightarrow {}^{13}C'$ coherence transfer in 2D and 3D NCA and NCO type chemical shift correlation experiments provide 35–60% higher transfer efficiencies than typical DCP-based alternatives while keeping the pulse sequence short and reducing the required rf field strengths by factors of 2–3. The latter is very important for biological applications where sample heating is a major issue of concern. The sensitivity gains result from improved robustness towards rf inhomogeneity and band-selective transfer between the spins of relevance. These features also render the optimal control experiments easy to setup relative to DCP and APCP experiments which are critically depending on the match between the two rf fields mutually and relative to the sample spinning frequency. We also demonstrated that the optimal control sequences, despite their many pulses with different amplitudes and phases, are not more susceptible to errors than conventional experiments. Actually, it proves to be exactly the opposite, the complexity of the experiments serves to compensate for many of the errors typically encountered in practical applications, as they are made part of the design requirements.

Obviously, the two experiments chosen in this study for demonstration of the applicability of optimal control experiment design in biological solid-state NMR do not

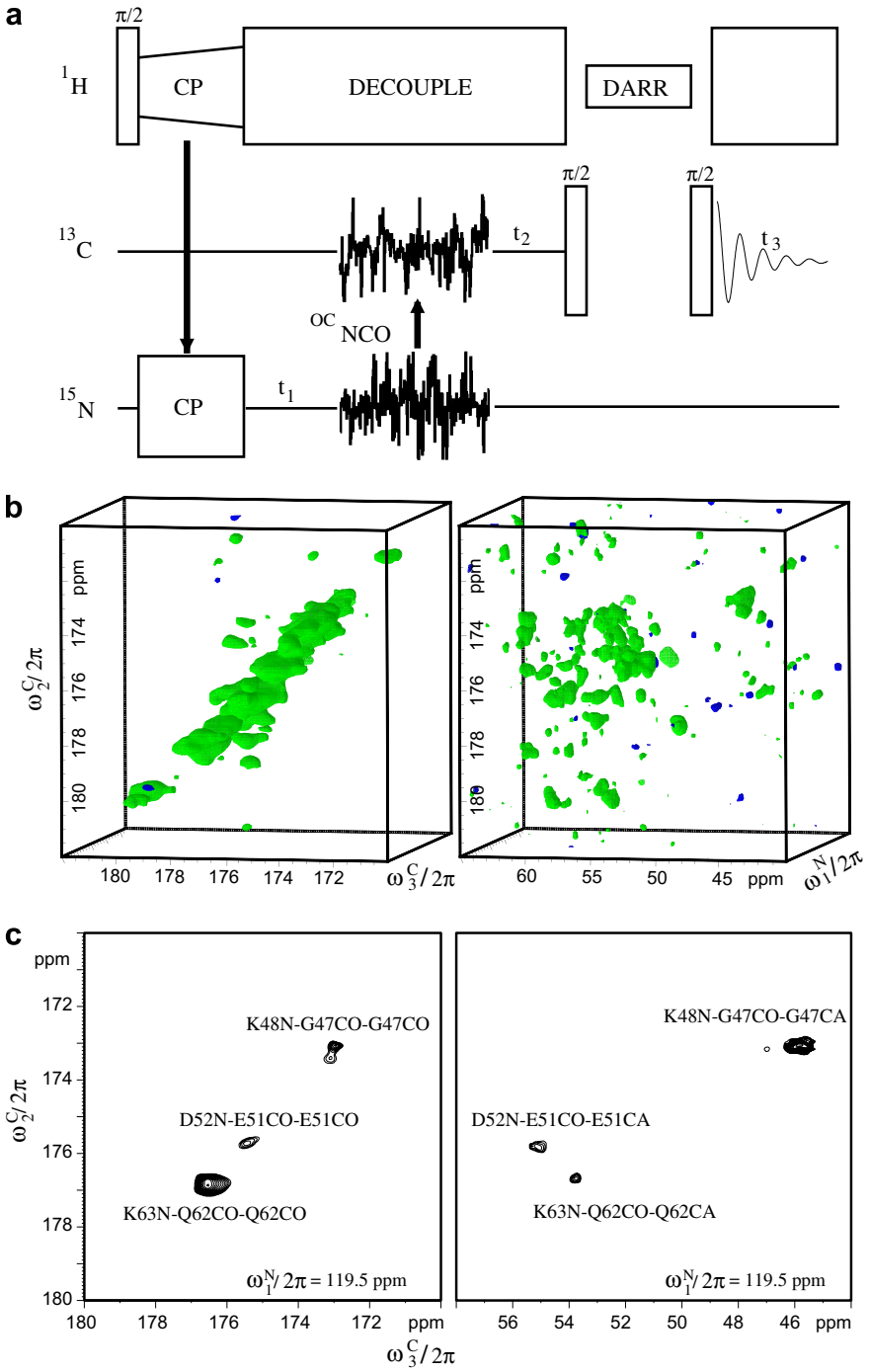

Fig. 10. 3D NCOCX experiments for uniformly ^{13}C,^{15}N-ubiquitin. (a) Schematic picture of the pulse sequence used for the experimental spectra in (b) and (c). (b) Carbonyl (left) and $^{13}C_\alpha$ (right) regions of a NCOCX experiments using the ^{OC}NCO optimal control optimized sequence in Fig. 2 for the ^{15}N to ^{13}C transfer. The ^{13}C′ to ^{13}CX transfer is carried out with a 30 ms DARR element with $\omega_H/2\pi = \omega_r/2\pi = 12$ kHz. (c) The ^{13}C′ (left) and $^{13}C_\alpha$ (right) regions of a 2D slice at $\omega_N/2\pi = 119.5$ ppm. Assignments of the individual peaks are indicated.

by any means fulfill the needs for all new and improved experiments. We foresee that similar improvements can be found for essentially all relevant coherence transfers, and that thereby optimal control pulse sequence elements will find their way into a majority of the pulse sequences presently used for biological solid-state NMR spectroscopy. This may be numerically derived pulse sequences, as presented here, or analytically derived "normal" pulse sequences designed with inspiration from the optimal control experiments.

Acknowledgments

We acknowledge support from the Danish National Research Foundation, the Danish Natural Science Foundation, Carlsbergfondet, and the Danish Biotechnology

Instrument Centre (DABIC). We are thankful to Dr. H. Thøgersen and Ms. I. Thøgersen for advice and support in expression and purification of ubiquitin and Stephan Grzesiek, University of Basel, Switzerland for providing us the plasmid. We thank Prof. A.E. McDermott and Dr. J.L. Lorieau, Columbia University, New York for helpful suggestions in relation to ubiquitin crystallization. We also thank Assoc. Prof. B. van Rossum for suggestions to the 3D experiments. S.J.G. thanks the DFG and the Fonds der Chemischen Industrie for support.

Appendix A. Supplementary data

Supplementary data associated with this article can be found, in the online version, at doi:10.1016/j.jmr.2007.06.011.

References

[1] F. Castellani, B. van Rossum, A. Diehl, M. Schubert, K. Rehbein, H. Oschkinat, Structure of a protein determined by solid-state magic-angle-spinning NMR spectroscopy, Nature 420 (2002) 98–102.
[2] A.T. Petkova, Y. Ishii, J.J. Balbach, O.N. Anzutkin, R.D. Leapman, F. Delaglio, R. Tycko, A structural model for Alzheimer's β-amyloid fibrils based on experimental constraints from solid-state NMR, Proc. Natl. Acad. Sci. USA 99 (2002) 16742–16747.
[3] S. Luca, J.F. White, A.K. Sohal, D.V. Filippov, J.H. van Boom, R. Grisshammer, M. Baldus, The conformation of neurotensin bound to its G protein-coupled receptor, Proc. Natl. Acad. Sci. USA 100 (2003) 10706–10711.
[4] C.P. Jaroniec, C.E. MacPhee, V.S. Bajaj, M.T. McMahon, C.M. Dobson, R.G. Griffin, High-resolution molecular structure of a peptide in an amyloid fibril determined by magic angle spinning NMR spectroscopy, Proc. Natl. Acad. Sci. USA 101 (2004) 711–716.
[5] A.T. Petkova, R.D. Leapman, Z.H. Guo, W.M. Yau, M.P. Mattson, R. Tycko, Self-propagating, molecular-level polymorphism in Alzheimer's β-amyloid fibrils, Science 307 (2005) 262–265.
[6] H. Heise, W. Hoyer, S. Becker, O.C. Andronesi, D. Reidel, M. Baldus, Molecular-level secondary structure, polymorphism, and dynamics of full-length alpha-synuclein fibrils studied by solid-state NMR, Proc. Natl. Acad. Sci. USA 102 (2005) 15871–15876.
[7] S.G. Zech, A.J. Wand, A.E. McDermott, Protein structure determination by high-resolution solid-state NMR spectroscopy: application to microcrystalline ubiquitin, J. Am. Chem. Soc. 127 (2005) 8618–8626.
[8] A. Lange, K. Giller, S. Hornig, M.F. Martin-Eauclaire, O. Pongs, S. Becker, M. Baldus, Toxin-induced conformational changes in a potassium channel revealed by solid-state NMR, Nature 440 (2006) 959–962.
[9] A.B. Siemer, C. Ritter, M.O. Steinmetz, M. Ernst, R. Riek, B.H. Meier, 13C, 15N resonance assignment of parts of the HET-s prion protein in its amyloid form, J. Biomol. NMR 34 (2006) 75–87.
[10] N. Ferguson, J. Becker, H. Tidow, S. Tremmel, T.D. Sharpe, G. Krause, J. Flinders, M. Petrovich, J. Berriman, H. Oschkinat, A.R. Fersht, General structural motifs of amyloid protofilaments, Proc. Natl. Acad. Sci. USA 103 (2006) 16248–16253.
[11] M. Etzkorn, M. Martell, O.C. Andronesi, K. Seidel, M. Engelhard, M. Baldus, Secondary structure, dynamics, and topology of a seven-helix receptor in native membranes, studied by solid-state NMR spectroscopy, Angew. Chem. Ingl. Ed. 46 (2006) 459–462.
[12] Y. Li, D.A. Berthold, H.L. Frericks, R.B. Gennis, C.M. Rienstra, Partial 13C and 15N chemical shift assignments of the disulfide-bond-forming enzyme DsbB by 3D magic-angle spinning NMR spectroscopy, ChemBioChem 8 (2007) 434–442.
[13] A. Goldbourt, B.J. Gross, L.A. Day, A.E. McDermott, Filamentous phage studied by magic-angle spinning NMR: resonance assignment and secondary structure of the coat protein in Pf1, J. Am. Chem. Soc. 129 (2007) 2338–2344.
[14] J. Schaefer, E.O. Stejskal, J.R. Garbow, R.A. McKay, Quantitative determination of the concentrations of C-13-N-15 chemical bonds by double cross-polarization NMR, J. Magn. Reson. 59 (1984) 150–156.
[15] M. Baldus, A.T. Petkova, J. Herzfeld, R.G. Griffin, Cross polarization in the tilted frame: assignment and spectral simplification in heteronuclear spin systems, Mol. Phys. 95 (1998) 1197–1207.
[16] G. Metz, X. Wu, S.O. Smith, Ramped-amplitude cross polarization in magic-angle-spinning NMR, J. Magn. Reson. A 110 (1994) 219–227.
[17] M. Baldus, D.G. Geurts, S. Hediger, B.H. Meier, Efficient N-15-C-13 polarization transfer by adiabatic-passage Hartmann–Hahn cross polarization, J. Magn. Reson. A 118 (1996) 140–144.
[18] M. Bjerring, N.C. Nielsen, Solid-state NMR heteronuclear coherence transfer using phase and amplitude modulated rf irradiation at the Hartmann–Hahn condition, Chem. Phys. Lett. 382 (2003) 671–678.
[19] M. Bjerring, J.T. Rasmussen, R.S. Krogshave, N.C. Nielsen, Heteronuclear coherence transfer in solid-state NMR using a γ-encoded transferred echo experiment, J. Chem. Phys. 119 (2003) 8916–8926.
[20] Y.K. Lee, N.D. Kurur, M. Helmle, O.G. Johannesen, N.C. Nielsen, M.H. Levitt, Efficient dipolar recoupling in the NMR of rotating solids. A seven-fold symmetric radiofrequency pulse sequence, Chem. Phys. Lett. 242 (1995) 304–309.
[21] M. Bjerring, N.C. Nielsen, Solid-state NMR heteronuclear dipolar recoupling using off-resonance symmetry-based pulse sequences, Chem. Phys. Lett. 370 (2003) 496–503.
[22] C.T. Kehlet, A.C. Sivertsen, M. Bjerring, T.O. Reiss, N. Khaneja, S.J. Glaser, N.C. Nielsen, Improving solid-state NMR dipolar recoupling by optimal control, J. Am. Chem. Soc. 126 (2004) 10202–10203.
[23] N. Khaneja, C. Kehlet, S.J. Glaser, N.C. Nielsen, Composite dipolar recoupling: anisotropy compensated coherence transfer in solid-state NMR, J. Chem. Phys. 124 (2006) 114503.
[24] N.C. Nielsen, H. Bildsøe, H.J. Jakobsen, M.H. Levitt, Double-quantum homonuclear rotary resonance: efficient dipolar recovery in magic-angle spinning NMR, J. Chem. Phys. 101 (1994) 1805–1812.
[25] A.W. Hing, S. Vega, J. Schaefer, Transferred-echo double-resonance NMR, J. Magn. Reson. 96 (1992) 205–209.
[26] J.R. Lewandowski, G. De Paepe, R. Griffin, Proton assisted insensitive nuclei cross polarization, J. Am. Chem. Soc. 129 (2007) 720–728.
[27] L. Pontryagin, B. Boltyanskii, R. Gamkrelidze, E. Mishchenko, The Mathematical Theory of Optimal Processes, Wiley-Interscience, New York, 1962.
[28] A. Bryson Jr., Y.-C. Ho, Applied Optimal Control, Hemisphere, Washington, DC, 1975.
[29] W.H. Press, S.A. Teukolsky, W.T. Vetterling, Numerical Recipes in C: The Art of Scientific Computing, Cambridge University Press, 1993.
[30] N. Khaneja, T. Reiss, C. Kehlet, T. Schulte-Herbrüggen, S.J. Glaser, Optimal control of coupled spin dynamics: design of NMR pulse sequences by gradient ascent algorithms, J. Magn. Reson. 172 (2005) 296–305.
[31] T. Reiss, N. Khaneja, S.J. Glaser, Time-optimal coherence-order-selective transfer of in-phase coherence in heteronuclear IS spin systems, J. Magn. Reson. 154 (2002) 192–195.
[32] N. Khaneja, T. Reiss, B. Luy, S.J. Glaser, Optimal control of spin dynamics in the presence of relaxation, J. Magn. Reson. 162 (2003) 311–319.
[33] N. Khaneja, J.-S. Li, C. Kehlet, B. Luy, S.J. Glaser, Broadband relaxation-optimized polarization transfer in magnetic resonance, Proc. Natl. Acad. Sci. USA 101 (2004) 14742–14747.
[34] K. Kobzar, B. Luy, N. Khaneja, S.J. Glaser, Pattern pulses: design of arbitrary excitation profiles as a function of pulse amplitude and offset, J. Magn. Reson. 173 (2005) 229–235.
[35] J.L. Neves, B. Heitmann, T.O. Reiss, H.H.R. Schor, N. Khaneja, S.J. Glaser, Exploring the limits of polarization transfer efficiency in homonuclear three spin systems, J. Magn. Reson. 181 (2006) 126–134.

[36] C. Kehlet, T. Vosegaard, N. Khaneja, S.J. Glaser, N.C. Nielsen, Low-power homonuclear dipolar recoupling in solid-State NMR developed using optimal control theory, Chem. Phys. Lett. 414 (2005) 204–209.
[37] T. Vosegaard, C. Kehlet, N. Khaneja, S.J. Glaser, N.C. Nielsen, Improved excitation schemes for multiple-quantum magic-angle spinning for quadrupolar nuclei designed using optimal control theory, J. Am. Chem. Soc. 127 (2005) 13768–13769.
[38] Z. Tosner, S.J. Glaser, N. Khaneja, N.C. Nielsen, Effective Hamiltonians by optimal control: solid-state NMR double-quantum and isotropic dipolar recoupling, J. Chem. Phys. 125 (2006) 184502.
[39] C. Kehlet, N.C. Nielsen, Solid-state NMR experiments by optimal control, Bruker Spin Report 157 (2007) 31–34.
[40] M. Bak, J.T. Rasmussen, N.C. Nielsen, SIMPSON: a general simulation program for solid-state NMR spectroscopy, J. Magn. Reson. 147 (2000) 296–330, Open source software, web-site www.bionmr.chem.au.dk..
[41] M. Bak, R. Schultz, T. Vosegaard, N.C. Nielsen, Specification and visualization of anisotropic interaction tensors for numerical simulation of solid-state NMR experiments on polypeptide structures, J. Magn. Reson. 154 (2002) 28–45, Open source software, web-site www.bionmr.chem.au.dk..
[42] F.C. Bernstein, T.F. Koetzle, G.J. Williams, E.E. Meier Jr., M.D. Brice, J.R. Rodgers, O. Kennard, T. Shimanouchi, M. Tasumi, The Protein Data Bank: a computer-based archival file for macromolecular structures, J. Mol. Biol. 112 (1977) 535–542.
[43] M. Bjerring, T. Vosegaard, A. Malmendal, N.C. Nielsen, Methodological development of solid-state NMR for characterization of membrane proteins, Concepts in Magnetic Resonance 18A (2003) 111–129.
[44] A.C. Sivertsen, M. Bjerring, C.T. Kehlet, T. Vosegaard, N.C. Nielsen, Numerical simulations in biological solid-state NMR spectroscopy, Ann. Rep. NMR Spectrosc. 54 (2005) 246–295.
[45] N.C. Nielsen, Computational aspects of biological solid-state NMR spectroscopy, in: A. Ramamoorthy (Ed.), Biological Solid-State NMR Spectroscopy, C. Dekker Inc., 2005, Chapter 6.
[46] R.H. Havlin, H. Le, D.D. Laws, A.C. de Dios, E. Oldfield, An ab initio quantum chemical investigation of carbon-13 NMR shielding tensorsin glycine, alanine, valine, isoleucine, serine, and threonine: Comparisons between helical and sheet tensors, and the effect of $\chi 1$ on shielding, J. Am. Chem. Soc. 119 (1997) 11951–11958.
[47] M. Hohwy, H.J. Jakobsen, M. Edén, M.H. Levitt, N.C. Nielsen, Broadband dipolar recoupling in the nuclear magnetic resonance of rotating solids: a compensated C7 pulse sequence, J. Chem. Phys. 108 (1998) 2686–2694.
[48] M. Hohwy, C.M. Rienstra, C.P. Jaroniec, R.G. Griffin, Fivefold symmetric homonuclear dipolar recoupling in rotating solids: application to double quantum spectroscopy, J. Chem. Phys. 110 (1999) 7983–7992.
[49] A. Brinkmann, M.H. Levitt, Symmetry principles in the nuclear magnetic resonance of spinning solids: heteronuclear recoupling by generalized Hartmann–Hahn sequences, J. Chem. Phys. 115 (2001) 357–384.
[50] E.H. Hardy, A. Detken, B.H. Meier, Fast-MAS total through-bond correlation spectroscopy using adiabatic pulses, J. Magn. Reson. 165 (2003) 208–218.
[51] M. Bak, N.C. Nielsen, REPULSION, A novel approach to efficient powder averaging in solid-state NMR, J. Magn. Reson. 125 (1997) 132–139.
[52] G. Drobny, A. Pines, S. Sinton, D. Weitekamp, D. Wemmer, Fourier transform multiple quantum nuclear magnetic resonance, J. Chem. Soc., Faraday Symp. 13 (1979) 49–60.
[53] K. Takegoshi, S. Nakamura, T. Terao, ^{13}C–^{1}H dipolar-assisted rotational resonance in magic-angle spinning NMR, Chem. Phys. Lett. 344 (2001) 631–637.
[54] R. Verel, M. Baldus, M. Ernst, B.H. Meier, A homonuclear spin-pair filter for solid-state NMR based on adiabatic-passage techniques, Chem. Phys. Lett. 287 (1998) 421–428.
[55] G. De Paëpe, M.J. Bayro, J. Lewandowski, R.G. Griffin, Broadband homonuclear correlation spectroscopy at high magnetic fields and MAS frequencies, J. Am. Chem. Soc. 128 (2006) 1776–1777.
[56] K. Seidel, M. Etzhorn, H. Heise, S. Becker, M. Baldus, High-resolution solid-state NMR studies of uniformly [^{13}C,^{15}N]-labeled ubiquitin, ChemBioChem 6 (2006) 1638–1647.
[57] T.I. Igumenova, A.E. McDermott, Homo-nuclear ^{13}C J-decoupling in uniformly ^{13}C-enriched solid proteins, J. Magn. Reson. 175 (2005) 11–20.